



ARTICLE

Bilevel Planning of Distribution Networks with Distributed Generation and Energy Storage: A Case Study on the Modified IEEE 33-Bus System

Haoyuan Li and Lingling Li*

State Key Laboratory of Reliability and Intelligence of Electrical Equipment, Hebei University of Technology, Tianjin, 300130, China

*Corresponding Author: Lingling Li. Email: lilingling@hebut.edu.cn

Received: 24 October 2024; Accepted: 03 February 2025; Published: 31 March 2025

ABSTRACT: Rational distribution network planning optimizes power flow distribution, reduces grid stress, enhances voltage quality, promotes renewable energy utilization, and reduces costs. This study establishes a distribution network planning model incorporating distributed wind turbines (DWT), distributed photovoltaics (DPV), and energy storage systems (ESS). K-means++ is employed to partition the distribution network based on electrical distance. Considering the spatiotemporal correlation of distributed generation (DG) outputs in the same region, a joint output model of DWT and DPV is developed using the Frank-Copula. Due to the model's high dimensionality, multiple constraints, and mixed-integer characteristics, bilevel programming theory is utilized to structure the model. The model is solved using a mixed-integer particle swarm optimization algorithm (MIPSO) to determine the optimal location and capacity of DG and ESS integrated into the distribution network to achieve the best economic benefits and operation quality. The proposed bilevel planning method for distribution networks is validated through simulations on the modified IEEE 33-bus system. The results demonstrate significant improvements, with the proposed method reducing the annual comprehensive cost by 41.65% and 13.98%, respectively, compared to scenarios without DG and ESS or with only DG integration. Furthermore, it reduces the daily average voltage deviation by 24.35% and 10.24% and daily network losses by 55.72% and 35.71%.

KEYWORDS: Distribution network planning; frank-copula joint output model; bilevel programming theory

1 Introduction

The electric power industry is the largest contributor to carbon emissions, exerting a significantly impacts on climate change [1]. DWT and DPV have emerged as preferred renewable energy sources due to their pollution-free nature and widespread distribution.

As commercial models and supportive legal policies for DG continue to evolve [2], the integration of DG into distribution networks becomes increasingly critical. This is particularly relevant in the context of rising electricity costs, the shift from traditional fossil fuels, and ongoing power supply challenges caused by inadequate transmission capacity [3]. DG integration provides several benefits, including localized energy utilization, deferral of network upgrades, and adaptability to specific local conditions, thus demonstrating significant potential for modern distribution networks [4].

Despite these advantages, traditional distribution networks face persistent issues such as low terminal voltage, high line losses, and significant reactive power consumption, driven by long supply lines and rapid load changes [5]. While DG integration can enhance voltage quality, optimize reactive power flow, and improve power supply reliability, irrational planning often results in challenges such as voltage rise at



connection points during peak renewable energy output and transformer overloads [6]. Furthermore, the intermittent and stochastic nature of DG exacerbates uncertainties in distribution network operations. These issues underscore the critical need for effective ESS to address the mismatch between peak DG output and load demand, smooth power output fluctuations, and reduce overall network losses [7].

Conventional methods for distribution network zoning, typically based on administrative or geographical boundaries, fail to capture electrical connectivity. Therefore, it is essential to incorporate electrical distance and power complementary characteristics during the planning stage to ensure a rational layout of DPV and ESS within the network. This approach enhances grid efficiency by mitigating local overloads and power imbalances [8].

To address DG output uncertainty, physical and statistical methods are commonly employed. Physical methods depend on weather forecasts and regional features but often yield complex and less generalizable models [9]. Statistical methods, including theoretical distribution models and kernel density estimation, have been widely used. However, these methods often depend on assumed distribution types [10], potentially leading to discrepancies between modeled and actual conditions. The Copula model, within statistical methods, offers high simulation accuracy and is suitable for diverse joint distributions, making it widely applicable in research on joint output models for wind and solar power [11]. Reference [12] proposed a methodology using multivariate Gaussian and Vine copulas to generate short-term scenarios of aggregated wind, photovoltaic, and small hydro production, evaluating their applications in reserve bidding and system scheduling. Reference [13] utilized the Frank-Copula function to generate output scenarios for wind and solar power in integrated energy systems. Case analyses indicated that scenarios simulated using this method exhibited distinct seasonal and temporal patterns, as well as correlations between wind and solar power daily outputs.

In distribution networks with numerous nodes, high DG penetration rates, small capacity, and dispersed interconnection points, the lack of unified planning during development has led to reverse overload conditions in regions with low power demand and weak supply capabilities. These overloads, occurring at specific times, severely exceed the distribution network's capacity, primarily due to arbitrary DG and ESS siting [14]. Predetermined candidate nodes often lack validation, leading to uneconomic operational states in certain areas or periods, thereby impacting the overall efficiency of the power system. Consequently, the selection of candidate nodes during planning is crucial [15]. Reference [16] identifies candidate nodes for DG deployment based on nodes with lower cost sensitivity factors. Tests conducted on IEEE 33-bus and 69-bus systems validate the method's effectiveness. However, the approach overlooks power-related impacts. From the perspective of improving operational reliability during planning, it is essential to enhance the complementarity and matching of power between nodes. Thus, this study opts to reflect electrical coupling relationships between nodes using electrical distance based on voltage-to-power sensitivity. In response to these challenges, this study proposes a comprehensive framework for distribution network planning that incorporates DG uncertainties, ESS integration, and power complementary characteristics to improve operational efficiency and reliability.

Distribution network planning can be approached using two main methodologies: traditional mathematical optimization techniques and artificial intelligence methods [17]. Traditional mathematical optimization typically begins with an initial solution, generated randomly or based on problem-specific characteristics within the solution space. This solution undergoes iterative updates using solving formulas until a predefined maximum number of iterations or convergence conditions are satisfied. Several models have been suggested for distribution network planning, such as the distributed robust optimization model [18], the mixed-integer quadratic constraint model [19], and the least-squares extrapolation technique [20].

In contrast to traditional mathematical optimization, based on artificial intelligence methods offer advantages in handling high-dimensional nonlinear problems inherent in distribution network planning, as they are less susceptible to local optimal [21]. Reference [22] proposed a hybrid genetic-particle swarm optimization method for optimal DG configuration. Reference [23] developed an algorithm that combines the non-dominated sorting genetic algorithm and tabu search, incorporating demand-side response for DG planning. The aforementioned studies did not incorporate ESS, limiting potential increases in DG penetration rates in distribution networks and resulting in low utilization of wind and PV power [24]. This study further develops a DG-ESS planning model that incorporates wind and solar power uncertainties with cluster partitioning, reformulated into a bilevel structure and solved using MIPSO for validation with the modified IEEE 33-bus system. The main contributions of this study are as follows:

- To address the uncertainties and correlations in wind and solar power outputs in distribution networks, a joint probability distribution model for DWT and DPV is established using the Frank-Copula function.
- To tackle the difficulty of determining the large number of DG and ESS grid-connected nodes in distribution networks, a cluster partitioning method based on electrical distance is proposed, effectively reducing the complexity of siting grid-connected nodes.
- A bilevel planning model for distribution networks incorporating DG and ESS is established, and a MIPSO algorithm adapted for mixed-integer programming is developed to efficiently solve the siting and sizing problems of DG and ESS, significantly improving the economic and operational performance of distribution networks.

The remaining sections are structured as follows: [Section 2](#) develops models for wind and solar uncertainties, as well as a distribution network clustering model, and presents the objective functions and constraints of the planning model. [Section 3](#) constructs a bilevel planning model for the distribution network. [Section 4](#) conducts simulation analyses using the modified IEEE 33-bus system, comparing four different scenarios. [Section 5](#) summarizes the research findings, conclusions, and prospects for future research.

2 Model Establishment

2.1 Simulation of Wind and Solar Uncertainty

Theoretical distribution models such as the Weibull and Beta distributions are employed to analyze the probability distribution of wind and solar power output [25]. However, these models necessitate precise parameter values, which are frequently unavailable. Kernel density estimation (KDE), a non-parametric approach, calculates the probability density function by placing a kernel function around each data point and computing the weighted average of these kernels. KDE offers flexibility by not assuming a specific data distribution a priori, thus enabling better adaptation to the data's inherent characteristics.

The KDE method assesses the influence of individual data points on the estimated value by comparing the distance between each data point and the point of interest. Data points in closer proximity to the point of interest are accorded greater weights, whereas those farther away receive diminished weights. Historical annual wind and solar power output data are organized into daily wind and solar power output samples as follows:

$$\begin{cases} X = \{X_1^1, X_1^2, \dots, X_1^{24}, X_2^1, X_2^2, \dots, X_2^{24}, \dots, X_{365}^1, X_{365}^2, \dots, X_{365}^{24}\} \\ Y = \{Y_1^1, Y_1^2, \dots, Y_1^{24}, Y_2^1, Y_2^2, \dots, Y_2^{24}, \dots, Y_{365}^1, Y_{365}^2, \dots, Y_{365}^{24}\} \end{cases} \quad (1)$$

For a specific point θ in the annual wind power output sample, the Gaussian function is used as the kernel function to estimate the density function $f(\theta)$ through kernel density estimation:

$$\hat{f}(\theta) = \frac{1}{nh_x\sqrt{2\pi}} \sum_{i=1}^n \exp\left(-\frac{1}{2}\left(\frac{\theta - X_i}{h_x}\right)^2\right) \quad (2)$$

where n is the sample size, and h_x is the bandwidth for WT kernel density estimation. The PV kernel density estimation is the same as Eq. (2).

The outputs of wind and solar power at a specific location display correlation alongside stochastic variability. Copula functions serve as versatile tools that connect the marginal distributions of multiple random variables to their joint distribution, effectively characterizing their correlation and dependence. In light of the observed negative correlation between wind and solar power, this study adopts the Frank Copula function to model their relationship:

$$F(x^t, y^t) = C_\lambda(F_{X^t}(x^t), F_{Y^t}(y^t)) \quad (3)$$

where $F_{X^t}(x^t)$ and $F_{Y^t}(y^t)$ are the marginal distribution functions of daily wind and solar power output, $F(x^t, y^t)$ is the joint distribution function of $F_{X_i}(x_i)$ and $F_{Y^t}(y^t)$, and $C_\lambda(\cdot)$ is the Frank Copula parameter controlling the correlation strength:

$$C_\lambda(u^t, v^t) = -\frac{1}{\lambda} \log\left(1 + \frac{(e^{-\lambda u^t} - 1)(e^{-\lambda v^t} - 1)}{e^{-\lambda} - 1}\right) \quad (4)$$

where $u = F_{X^t}(x^t)$, $v = F_{Y^t}(y^t)$, and λ is a parameter of the Copula that controls the strength of the correlation.

Eq. (4) is substituted into Eq. (3) to establish the joint probability distribution function. Random sampling from this joint distribution function across each time period, followed by inverse transformation of these samples, produces comprehensive daily data on wind and solar power outputs. This approach captures both the correlation and stochastic nature inherent in these renewable energy sources. Finally, typical daily scenarios of wind and solar power outputs are generated using the K-means clustering method.

2.2 Cluster Partitioning of Distribution Networks

The partitioning of distribution network clusters is typically based on electrical distance, defined by the sensitivity relationship between voltage magnitude and injected power. The voltage magnitude-power sensitivity can be derived from the Newton-Raphson polar coordinate power flow correction equation:

$$\begin{bmatrix} \Delta P \\ \Delta Q \end{bmatrix} = \begin{bmatrix} J_{P\theta} & J_{PU} \\ J_{Q\theta} & J_{QU} \end{bmatrix} \begin{bmatrix} \Delta\theta \\ \Delta U \end{bmatrix} \quad (5)$$

Considering the distribution network is shorter in distance and has a relatively uniform load compared to the transmission network, changes in voltage magnitude are more significant than changes in voltage phase. Therefore, $\Delta\theta$ is omitted:

$$\Delta U = S_{UP}\Delta P + S_{UQ}\Delta Q = (J_{PU} - J_{P\theta}J_{Q\theta}^{-1}J_{QU})^{-1}\Delta P + (J_{QU} - J_{Q\theta}J_{P\theta}^{-1}J_{PU})^{-1}\Delta Q \quad (6)$$

In the distribution network, variations in both active and reactive power affect voltage, necessitating their inclusion in the electrical distance calculation. The coefficient D_{ij} , which represents the overall impact

of changes in the injected power at node i on the voltage magnitude at node j , is defined based on S_{UP} and S_{UQ} as shown in Eq. (7):

$$D_{ij} = S_{UP_{ii}} - S_{UP_{ij}} + S_{UQ_{ii}} - S_{UQ_{ij}} \quad (7)$$

where $S_{UP_{ii}}$ and $S_{UP_{ij}}$ are elements of the S_{UP} matrix, indicating the impact of changes in active power injection at nodes i and j on the voltage magnitude at node i , respectively. Similarly, $S_{UQ_{ii}}$ and $S_{UQ_{ij}}$ are elements of the S_{UQ} matrix, indicating the impact of changes in reactive power injection at nodes i and j on the voltage magnitude at node i , respectively.

$$L_{ij} = L_{ji} = \sqrt{\sum_{l=1}^n (D_{il} - D_{jl})^2} \quad (8)$$

where n is the total number of nodes in the distribution network, and L_{ij} represents the electrical distance between node i and node j .

After calculating the electrical distances between all nodes, clustering is conducted using the K-means algorithm. The traditional K-means algorithm randomly selects initial cluster centers, which can result in convergence to a local optimum. To address this, the K-means++ algorithm is employed, selecting high-density nodes as initial cluster centers to enhance the selection process.

For each node, M nearest neighbors are chosen. If M is too large, the algorithm may converge to a local optimum due to overly concentrated initial cluster centers from high-density nodes. Conversely, if M is too small, the initial cluster centers may lack diversity, leading to significant deviation in clustering outcomes. Experimental iterations demonstrate that an optimal selection of M enhances clustering performance.

The sum of the electrical distances between each node i and its nearest M nodes is calculated as shown in Eq. (10):

$$LS_i = \{LS_1, LS_2, \dots, LS_N\} \quad (9)$$

These sums are arranged in ascending order, with the top k nodes identified as high-density nodes. These nodes are selected as the initial cluster centers in the K-means++ algorithm. The objective function for K-means++ clustering is the sum of the squared electrical distances between nodes within each cluster and the central node, as shown in Eq. (10):

$$J = \min \sum_{k=1}^m \sum_{i=1}^{N_k} L_{i\gamma_k}^2 \quad (10)$$

where m is the number of clusters in the distribution network, N_k is the number of nodes in the k -th cluster, and γ_k is the node with the minimum electrical distance to other nodes in the k -th cluster, serving as the central node of the k -th cluster.

2.3 Objective Function

2.3.1 Upper-Layer Planning Model

Annual comprehensive cost of the distribution network:

$$F_{upp} = F_{op} + F_{in} + F_{buy} + F_{loss} + F_{sub} \quad (11)$$

Annual operational costs:

$$F_{op} = F_{op}^{DG} + F_{op}^{ESS} \quad (12)$$

where F_{op}^{DG} and F_{op}^{ESS} are the annual operational costs of DG and ESS, respectively.

$$F_{op}^{DG} = \sum_{s=1}^{M_s} \eta_s \sum_{t=1}^{24} (\varphi_{WT} P_{s,t}^{WT} + \varphi_{PV} P_{s,t}^{PV}) \quad (13)$$

where φ_{WT} and φ_{PV} are the operating costs of wind power and PV power, $P_{s,t}^{WT}$ and $P_{s,t}^{PV}$ are the actual outputs of wind power and PV power at time t under scenario s , M_s is the number of typical scenarios divided into one year, and η_s is the probability of the scenario.

$$F_{op}^{ESS} = \sum_{s=1}^{M_s} \eta_s \sum_{t=1}^{24} (\varphi_{ESS} (P_{ch,s,t}^{ESS} + P_{dch,s,t}^{ESS})) \quad (14)$$

where φ_{ESS} is the operating cost of energy storage, and $P_{ch,s,t}^{ESS}$ and $P_{dch,s,t}^{ESS}$ are the power of energy storage charging and discharging at time t under scenario s .

Annual Equivalent Investment Costs:

$$\begin{cases} F_{in} = F_{in}^{PV} + F_{in}^{WT} + F_{in}^{ESS} \\ F_{in}^{WT} = C_{WT} \sum_{k=1}^m P_{k,WT} \frac{r(1+r)^{n_1}}{(1+r)^{n_1}-1} \\ F_{in}^{PV} = C_{PV} \sum_{k=1}^m P_{k,PV} \frac{r(1+r)^{n_2}}{(1+r)^{n_2}-1} \\ F_{in}^{ESS} = C_{ESS} \sum_{k=1}^m P_{k,ESS} \frac{r(1+r)^{n_3}}{(1+r)^{n_3}-1} \end{cases} \quad (15)$$

where C_{WT} , C_{PV} and C_{ESS} are the unit capacity investment costs of WT, PV and ESS, respectively, r is the discount rate, and n_1 , n_2 and n_3 are the service lives of WT, PV, and ESS, respectively.

Costs of Interaction with the Upper-Level Grid:

$$F_{grid} = F_{buy} - R_{sell} \quad (16)$$

where F_{buy} represents the cost of purchasing electricity from the upper-level grid, and R_{sell} represents the revenue from selling electricity back to the upper-level grid.

$$F_{buy} = \sum_{s=1}^{M_s} \eta_s \sum_{t=1}^{24} E_t^{buy} P_{t,s}^{grid_buy} \quad (17)$$

where E_t^{buy} is the grid electricity price at time t , and $P_{t,s}^{grid_buy}$ is the amount of electricity purchased from the main grid at time t in scenario s .

$$R_{sell} = \sum_{s=1}^{M_s} \eta_s \sum_{t=1}^{24} E_t^{sell} P_{t,s}^{grid_sell} \quad (18)$$

where E_t^{sell} is the power purchase price of the power grid at time t , $P_{t,s}^{grid_sell}$ is the amount of electricity returned to the main grid at time t under scenario s .

Unlike the current DG generation benefits which already cover costs and with subsidies gradually phasing out, the ESS profit mechanism is not yet perfected and the price of ESS remains high. Hence, subsidies are required for ESS generation [26].

Subsidies for ESS generation are typically structured as capacity price subsidies:

$$F_{sub} = \sum_{s=1}^{M_s} \eta_s \sum_{t=1}^{24} E_{t,sub} P_{dch,s,t}^{ESS} \quad (19)$$

where $E_{t,sub}$ is the capacity price at time t .

2.3.2 Lower-Level Operation and Control Model

The objective function is the sum of the annual network loss cost and the voltage fluctuation penalty coefficient:

$$F_{low} = F_{loss} + F_V \quad (20)$$

Annual network loss cost:

$$F_{loss} = \varphi_{loss} \sum_{s=1}^{M_s} \eta_s \sum_{t=1}^{24} P_{t,s}^{loss} \quad (21)$$

where φ_{loss} is the network loss discounting cost coefficient, and $P_{t,s}^{loss}$ is the system network loss power at moment t under scenario s .

Annual voltage fluctuation penalty costs:

$$F_V = \varphi_V \sum_{s=1}^{M_s} \eta_s \sum_{t=1}^{24} \sum_{i=1}^N |V_{s,t,i} - 1| \quad (22)$$

where φ_V is the voltage fluctuation penalty factor, and $V_{s,t,i}$ is the voltage amplitude at node i at moment t under scene s .

2.4 Decision Variables

$$x = \left\{ \begin{matrix} a_1^{WT}, \dots, a_i^{WT}, \dots, a_m^{WT}, u_1^{WT}, \dots, u_i^{WT}, \dots, u_m^{WT} \\ a_1^{PV}, \dots, a_i^{PV}, \dots, a_m^{PV}, u_1^{PV}, \dots, u_i^{PV}, \dots, u_m^{PV} \\ a_1^{ESS}, \dots, a_i^{ESS}, \dots, a_m^{ESS}, u_1^{ESS}, \dots, u_i^{ESS}, \dots, u_m^{ESS} \end{matrix} \right\} \quad (23)$$

where a_i^{WT} , a_i^{PV} , a_i^{ESS} are the access locations of wind energy storage in the i -th cluster, and u_i^{WT} , u_i^{PV} , u_i^{ESS} are the wind energy storage capacities of the corresponding access locations.

2.5 Constraints

2.5.1 Maximum Node Access DG Capacity

$$0 \leq P_{DG_i} \leq P_{DG_i}^{\max} \quad (24)$$

where P_{DG_i} is the capacity of node i to access the DG, $P_{DG_i}^{\max}$ and is the maximum value of the capacity of node i allowed to access the DG.

2.5.2 Node Maximum Access ESS Capacity

$$0 \leq P_{ESS_i} \leq P_{ESS_i}^{\max} \quad (25)$$

where P_{ESS_i} is the capacity of node i to access the DG, and $P_{ESS_i}^{\max}$ is the maximum value of the capacity of node i allowed to access the DG.

2.5.3 DG Installed Penetration Constraints

$$\sum_{k=1}^m P_{k,DG} \leq \psi P_{load} \quad (26)$$

where $P_{k,DG}$ is the planning capacity of DG in k clusters, P_{load} is the total system load, and ψ is the maximum new energy penetration rate of the system.

2.5.4 Nodal Voltage Constraints

$$U_i^{\min} \leq U_i \leq U_i^{\max} \quad (27)$$

where U_i is the voltage amplitude at node i , U_i^{\max} and U_i^{\min} are the upper and lower limits of the voltage at node i .

2.5.5 Node Power Constraints

$$\begin{cases} \Delta P_i = U_i \sum_{j \in N_i} U_j (G_{ij} \cos \theta_{ij} + B_{ij} \sin \theta_{ij}) \\ \Delta Q_i = U_i \sum_{j \in N_i} U_j (G_{ij} \sin \theta_{ij} - B_{ij} \cos \theta_{ij}) \end{cases} \quad (28)$$

where ΔP_i and ΔQ_i denote the active and reactive power injected by node i , respectively, G_{ij} and B_{ij} denote the conductance between nodes i and j , and N_i is the number of nodes connected to node i .

2.5.6 Branch Transmission Power Constraints

$$0 \leq S_l \leq S_l^{\max} \quad (29)$$

where S_l is the transmission power of branch l , and S_l^{\max} is the limit value of the transmission power of branch l .

3 Model Optimization Methods and Solutions

3.1 Establishment and Solution of the Bilevel Model

Bilevel programming offers a structured approach for tackling intricate problems by dividing them into upper and lower levels. This hierarchical framework is employed to optimize system-wide issues. Each level is characterized by its own objective functions, decision variables, and constraints. The upper and lower levels are interlinked and collaboratively iterated to achieve the optimal solution.

In this study, the upper-level model focuses on minimizing the system's annual comprehensive cost while determining the optimal locations and capacities of DG and ESS, these optimal configurations are

fed into the lower-level model. The lower-level model is designed to minimize annual network losses and penalties associated with voltage fluctuations. Fig. 1 depicts the process of establishing and solving the bilevel model for the system.

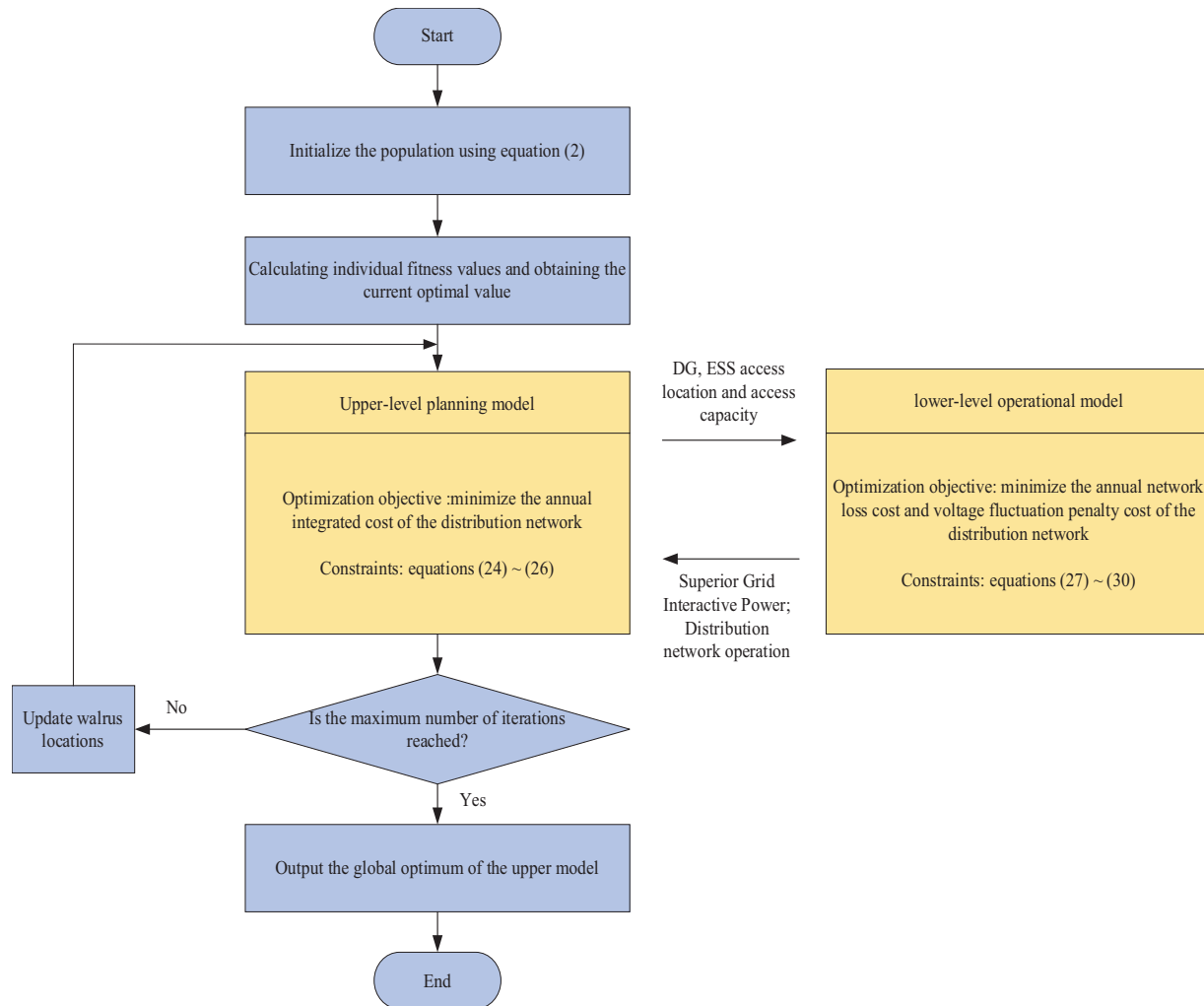


Figure 1: Distribution network two-layer planning model

The bilevel programming model links its two layers through transfer variables. The upper-level model functions as the leader, emphasizing economic benefits, while the lower-level model focuses on system operational quality. Network loss costs represent the distribution of power flows within the system, and voltage fluctuation penalty costs denote voltage variations.

The upper-level planning model first determines the decision variable x , which it then transfers to the lower-level operational model. Utilizing a second-order cone relaxation programming approach [27], the lower-level model computes the optimal power flow solution and communicates the results back to the upper-level model. These outcomes are subsequently integrated into the upper-level model's objective function solving process. This iterative procedure continues until a global optimal solution is attained or the maximum number of iterations is reached.

Throughout the solving process, bilevel programming accounts for both the economic objectives of the upper level and the operational objectives of the lower level. The two models mutually constrain and influence each other, ultimately achieving an optimal solution that satisfies both sets of objectives. This method not only maximizes economic benefits but also ensures high system operational quality, providing substantial practical application value.

3.2 Mixed-Integer Particle Swarm Optimization Algorithm

To address the mixed-integer nonlinear characteristics of distribution network planning problems, this study introduces a MIPSO designed for mixed-integer optimization. The proposed MIPSO employs a dimension-separated update strategy to accommodate the distinct characteristics of continuous and integer variables. Decision variables are divided into continuous and integer subsets, with tailored update rules for each subset.

In mixed-integer optimization problems, integer variables must be discretized to ensure solution feasibility while maintaining the convergence properties of continuous variables. For integer variable optimization, genetic algorithm (GA) operations, including selection, crossover, and mutation, are integrated into the particle update process. In this algorithm, the decision variables of the i -th particle are defined as:

$$X_i = \{X_i^{(C)}, X_i^{(I)}\} \quad (30)$$

where $X_i^{(C)}$ denotes the continuous variable, which is updated using the PSO algorithm [28], $X_i^{(I)}$ represents the integer variable, updated through the crossover and mutation mechanisms of the genetic algorithm [29]. The processing flow is illustrated in the Fig. 2.

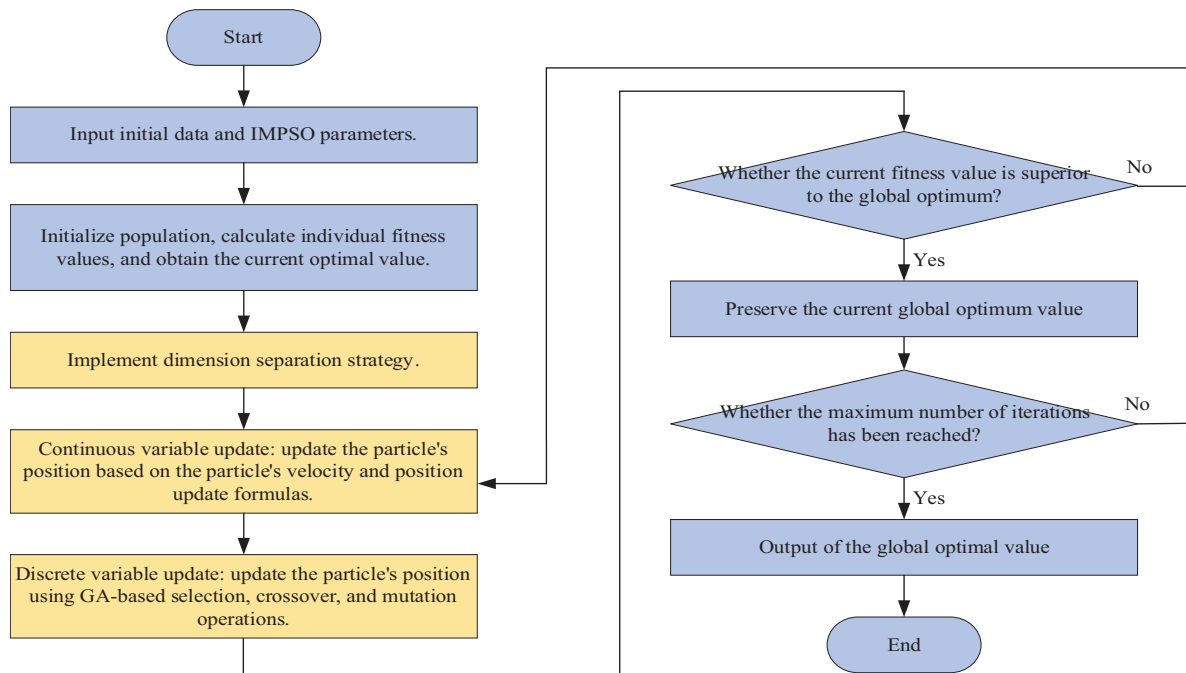


Figure 2: Mixed-integer particle swarm optimization algorithm flow chart

4 Case Analysis

4.1 WT and PV Output Scenario Clustering

Data on WT and PV output from a region in North China in 2022 were utilized for this study, with per-unit values illustrated in Fig. 3. Employing the scenario generation method detailed in Section 2.1, both the WT window width h_x and the PV window width h_y were set to 0.05. This process yielded 1000 sets of typical daily per-unit values for wind and solar output, subsequently grouped into four distinct daily scenarios for wind and solar output using the k-means algorithm. Fig. 4 is the Frank-Copula distribution function graph for the WT and PV outputs.

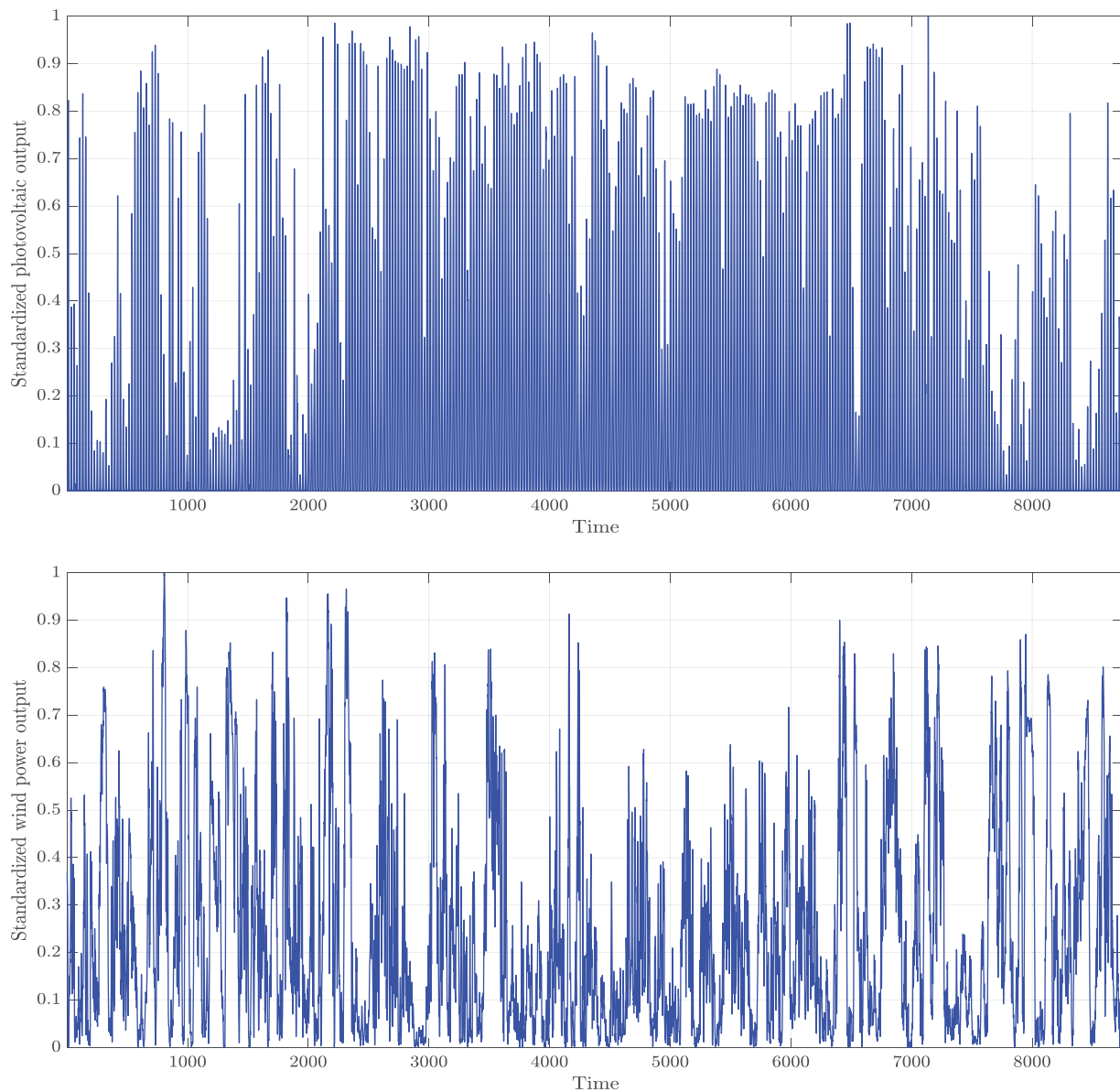


Figure 3: Historical output of PV and WT in a certain region in 2022

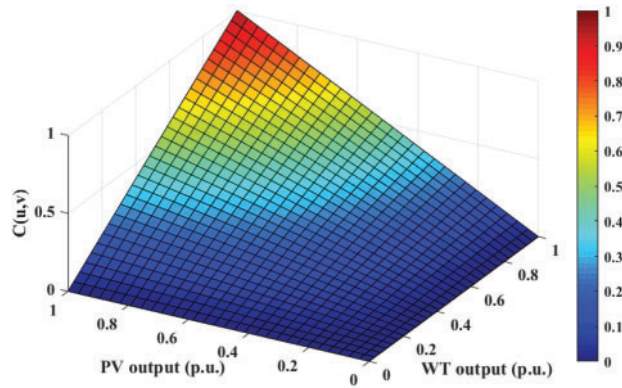


Figure 4: Frank-Copula distribution function graph

In Fig. 5, WT output appears more consistent across all scenarios. At night, as surface temperatures drop, atmospheric temperature differentials increase, fostering brisk air movement that boosts power generation, partially offsetting PV output. Within each scenario, wind and solar outputs show correlations, sometimes exhibiting consistent or opposing trends in specific periods. For instance, in Scenario 2, both wind and solar outputs decrease around noon due to intense summer heat, which stifles wind and hampers PV generation. Seasonal differences between scenarios are pronounced, reflecting distinct seasonal patterns. In Scenario 4, diminished solar irradiance during winter and earlier sunsets result in notably reduced PV output compared to other scenarios, aligning with the quarterly output trough evident in January, February, and December in Fig. 3.

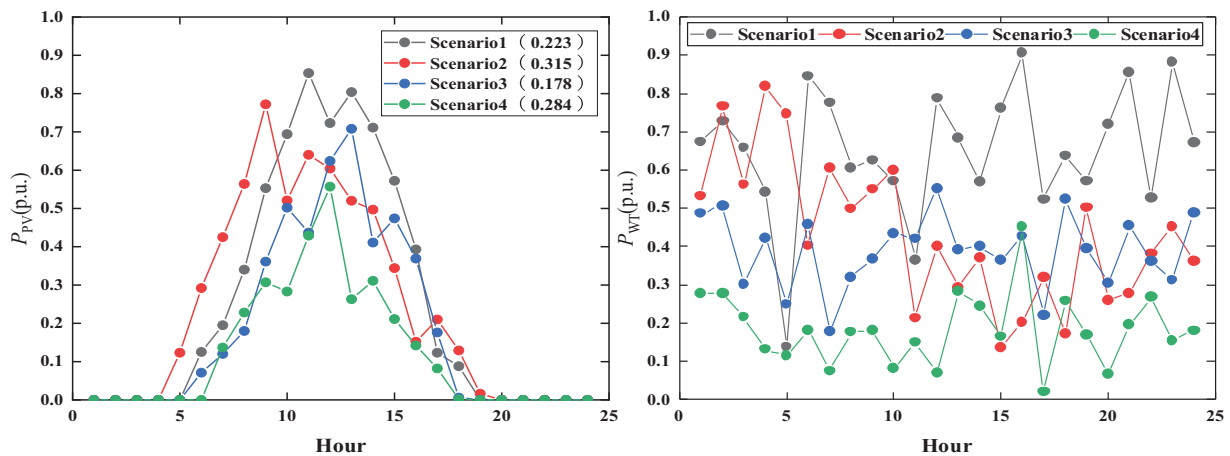


Figure 5: scenario generation results

4.2 Cluster Partitioning of IEEE 33-Bus System

The study focused on the modified IEEE 33-bus system, featuring an active load of 37.15 MW, a reactive load of 23 MW, and a system reference voltage set at 12.66 kV. Employing the K-means++ algorithm, the distribution system was segmented into clusters according to electrical distance. Fig. 6 illustrates the outcomes of cluster partitioning across various K values.

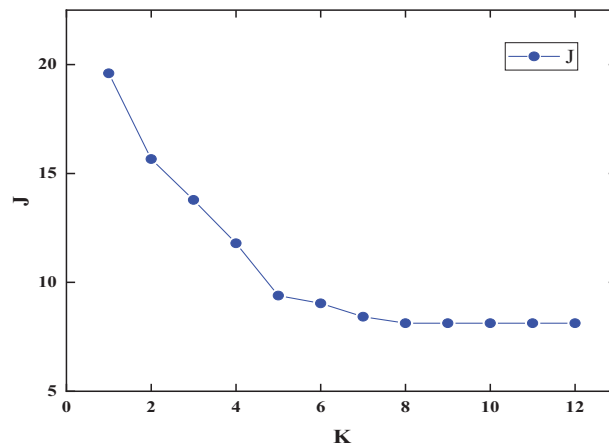


Figure 6: Partitioning indicators under different numbers of clusters

The optimal number of clusters K was determined using the elbow method [30]. Fig. 6 clearly indicates that $K = 5$ represents a significant inflection point. Given the structure of the distribution network, five clusters were chosen for partitioning, as illustrated in Fig. 7.

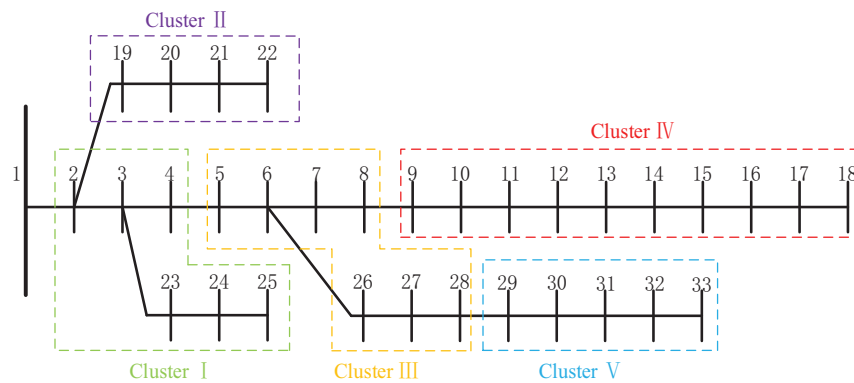


Figure 7: Distribution network division structure diagram

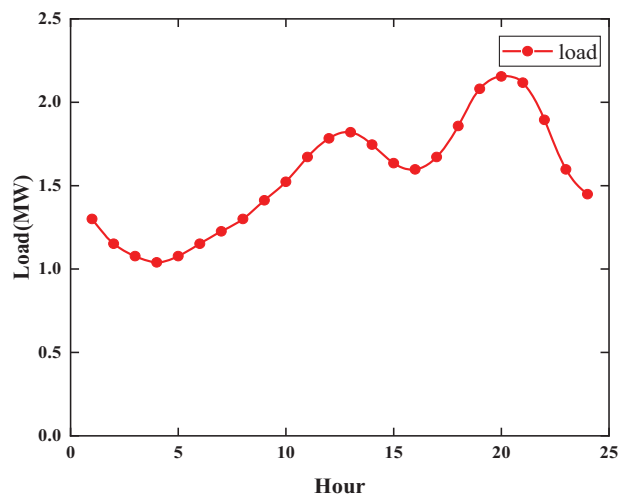
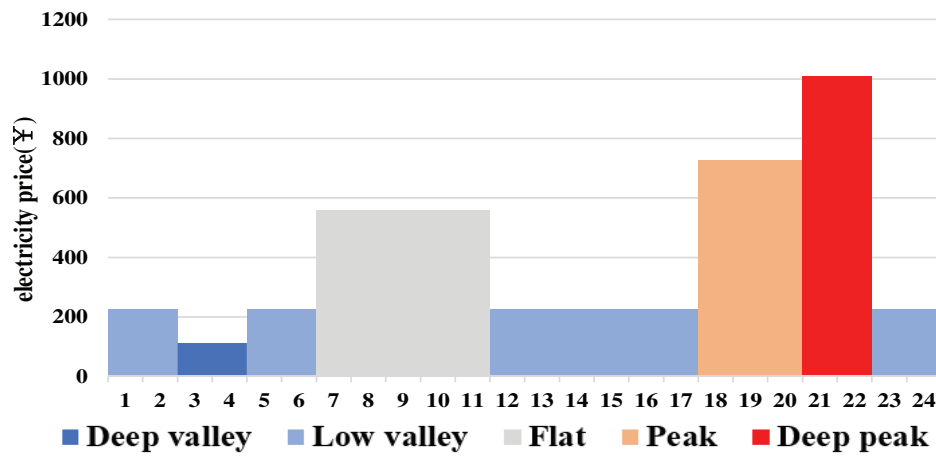
4.3 IEEE 33-Bus System Parameters and Optimization Settings

The system is permitted to export electricity to the main grid, with exported electricity priced at 70% of the prevailing electricity rate. Table 1 outlines additional key parameters of the system. The power distribution ratios for individual load nodes are configured using default settings, and fluctuations in system load over time are depicted in Fig. 8.

The base electricity price under peak-valley tariffs is ¥560/MW. The coefficients for periods of deep valley, low valley, flat periods, high peak, and deep peak are 0.2, 0.4, 1, 1.3, and 1.8 times the base price, respectively, as depicted in Fig. 9.

Table 1: System parameter

Parameters	Value
Maximum DG installed capacity penetration (p.u.)	120%
Maximum transmission power of the line (MVA)	3
Maximum return power (MVA)	2
Network loss cost coefficient (¥/MVA)	200
Voltage fluctuation penalty coefficient (¥/(p.u. h))	10
Node voltage amplitude (p.u.)	0.95~1.05

**Figure 8:** System daily load fluctuation diagram**Figure 9:** System daily peak and valley electricity price

Based on the relatively short spatiotemporal distances within the distribution network in the same region, the DG output characteristics are assumed to be uniform. To minimize the lifespan reduction of the ESS caused by deep discharges and high-power charge/discharge cycles [31], the minimum ESS charge level is set at 10% of its capacity, with the charge/discharge efficiency limited to 30% of the capacity. Additionally, the compensation price for ESS capacity follows peak and off-peak electricity prices, with a base rate of ¥100/MW. The key parameters of both DG and ESS systems are detailed in Table 2.

Table 2: DG, ESS parameters

Parameter	WT	PV	ESS
Service life	15	20	16
Discount rate	0.06	0.06	0.06
Investment cost	8500	6500	1500
Operation and maintenance cost	0.03	0.03	0.015

The maximum number of iterations in the MIPSO algorithm is set to 100. For continuous variable optimization, the number of particles is set to 30, the learning parameters C_1 and C_2 are both 2, the maximum value of the inertia weight w is 0.9, and the minimum value is 0.1, the dimensionality is set to 15, corresponding to the capacities of DPV, DWT, and ESS in the five clusters. For integer variable optimization, the population size remains 30, the crossover probability is 0.8, and the mutation probability is 0.05, the dimensionality is also set to 15, corresponding to the locations of PV, WT, and ESS in the five clusters.

4.4 Economic Evaluation of Planning Results

Each cluster in the model is configured to include one access point for DWT, DPV, and ESS, respectively, allowing multiple devices to connect to the same node. The access capacity for DWT and DPV at each node is limited to 100–500 kW, while ESS access is restricted to 100–700 kW. Table 3 shows the DG and ESS planning results of each cluster after MIPSO solution.

Table 3: Planning results under MIPSO

Cluster	WT ^{bus} (KW)	PV ^{bus} (KW)	ESS ^{bus} (KW)	Fitness
I	450.2 ^{3}	176.2 ^{4}	522.8 ^{23}	413.257E – 04
II	500.0 ^{21}	232.4 ^{22}	190.6 ^{22}	
III	321.2 ^{26}	323.2 ^{7}	441.5 ^{8}	
IV	331.9 ^{11}	246.7 ^{12}	589.6 ^{16}	
V	380.8 ^{33}	314.6 ^{33}	596.7 ^{30}	

Table 3 presents planning outcomes applied to the modified IEEE 33-bus system. DWT capacities generally exceed those of DPV. This disparity arises because DWT, despite a slightly higher unit cost than DPV, offers longer daily generation durations, thereby delivering superior overall daily generation benefits.

In terms of cluster analysis, Cluster II exhibits the highest DG planning capacity, facilitated by its ability to inject electricity back into the upstream grid, thereby reducing network losses compared to other clusters. Within clusters, DG capacity correlates positively with ESS capacity. This relationship emerges because

surplus DG generation within clusters tends to be absorbed internally by the system. The topology diagram of the planning results in Table 3 is shown in Fig. 10.

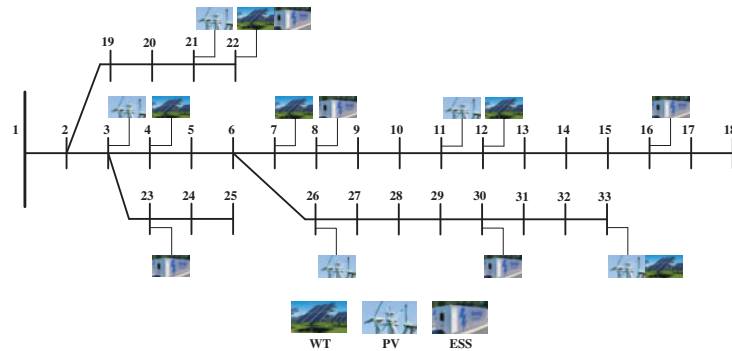


Figure 10: Modified IEEE 33-bus system DG-ESS planning diagram under MIPSO

The operational performance of the modified IEEE 33-bus distribution network is assessed based on economic benefits and power quality considerations. Four scenarios are examined to validate the efficacy of the proposed model:

Case1: No installation of DG or ESS.

Case2: Installation of DG using the algorithm and model proposed herein, without ESS.

Case3: Installation of DG and ESS using the algorithm and model proposed herein, without accounting for the compensation price for energy storage capacity.

Case 4: Installation of DG and ESS using the algorithm and model proposed herein, accounting for the compensation price for energy storage capacity.

Table 4 demonstrates that deploying DG effectively reduces the operational costs of the distribution network. In Case2, annual comprehensive costs decrease by 32.17% compared to Case1, with DG benefits covering its construction costs, indicating substantial economic gains. This reduction is attributed to declining DG unit prices over recent decades due to technological advancements. In Case4, compared to Case1, annual comprehensive costs decrease by 41.65%, indicating that the combined integration of DG and ESS achieves higher economic benefits than the sole integration of DG. In Case3, annual comprehensive costs decrease by 4.50% compared to Case2, primarily because ESS are relatively new, with their unit prices still requiring further market development. Presently, profitability from energy storage based solely on peak-valley arbitrage barely offsets costs. In Case4, annual comprehensive costs decrease by 9.92% compared to Case3, attributed to subsidies for energy storage capacity prices. Additionally, introducing energy storage capacity pricing increases energy storage penetration rates by 52.72%.

Table 4: Planning results under the four scenarios

Case	Cluster	WT ^{bus} (KW)	PV ^{bus} (KW)	ESS ^{bus} (KW)	Fitness
Case1	I	—	—	—	708.238E – 06
	II	—	—	—	
	III	—	—	—	
	IV	—	—	—	
	V	—	—	—	

(Continued)

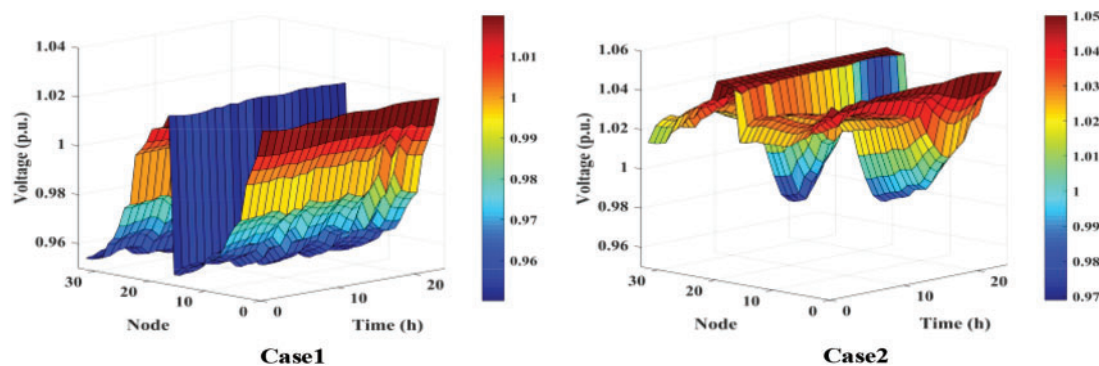
Table 4 (continued)

Case	Cluster	WT ^{bus} (KW)	PV ^{bus} (KW)	ESS ^{bus} (KW)	Fitness
Case2	I	293.7 ^{25}	215.6 ^{4}	–	480.399E – 06
	II	380.0 ^{21}	149.1 ^{22}	–	
	III	364.5 ^{28}	100.0 ^{8}	–	
	IV	258.6 ^{14}	235.3 ^{11}	–	
	V	401.2 ^{33}	259.4 ^{31}	–	
Case3	I	376.2 ^{3}	224.1 ^{4}	169.6 ^{23}	458.764E – 06
	II	415.5 ^{21}	100 ^{21}	291.6 ^{22}	
	III	199.3 ^{26}	347.2 ^{7}	179.1 ^{7}	
	IV	231.4 ^{11}	350 ^{13}	393.5 ^{14}	
	V	410.3 ^{32}	323.3 ^{33}	499.2 ^{33}	
Case4	I	450.0 ^{3}	176.2 ^{4}	522.8 ^{23}	413.257E – 06
	II	500.0 ^{21}	132.4 ^{22}	190.6 ^{22}	
	III	321.2 ^{26}	323.2 ^{7}	441.5 ^{8}	
	IV	331.9 ^{11}	346.7 ^{12}	589.6 ^{16}	
	V	380.8 ^{33}	414.6 ^{33}	596.7 ^{30}	

4.5 Operational Quality Analysis of Planning Results

The operational quality analysis of the distribution network in this study focuses on power quality and network loss levels. Fig. 11 illustrates the three-dimensional voltage distribution on a typical summer day across the four scenarios. Table 5 details daily voltage deviations and network losses for these scenarios.

Fig. 11 illustrates that in Case1, without DG and ESS, there are notable voltage fluctuations across distribution network nodes. Only nodes close to the upstream main grid maintain voltage around 1.00 p.u., while most end nodes experience low voltage. In Case2, introducing DG resolves low voltage issues at end nodes, yet excessive DG causes overvoltage at installation sites and nearby nodes. Case3 shows that installing DG and ESS concurrently effectively mitigates DG-induced overvoltage, resulting in smoother voltage fluctuations across the network. In Case4, with higher DG and ESS penetration than Case3, overall voltage fluctuation reduction is modest, but localized areas experience more pronounced voltage stabilization.

**Figure 11:** (Continued)

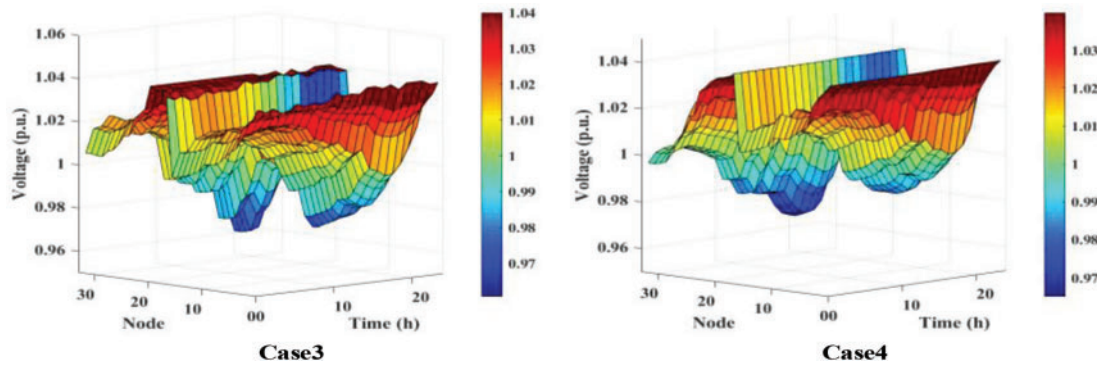


Figure 11: Typical summer daily voltage distribution under four cases

Table 5 illustrates that Case2 exhibits a 17.06% reduction in daily voltage deviation compared to Case1, accompanied by a 31.13% decrease in network losses. This installation of DG effectively enhances node voltage and optimizes internal power flow within the distribution network. In Case3, voltage values range from approximately 0.96 to 1.04 p.u., indicating improved node power supply quality. In Case4, the daily voltage deviation and network losses are the lowest, with reductions of 24.35% and 55.72%, respectively, compared to Case1. This highlights that appropriate ESS subsidies promote energy storage market growth and larger ESS capacities effectively mitigate voltage fluctuations and reduce power company losses due to network inefficiencies.

Table 5: Daily average voltage deviation and daily average network loss under the four scenarios

Case	Daily voltage fluctuation (p.u. h)	Daily network loss (MW)
Case1	28.408	2.281
Case2	23.563	1.571
Case3	21.907	1.096
Case4	21.149	1.010

5 Concluding Remarks

In response to escalating climate change from excessive carbon emissions, integrating DG and ESS into the grid at large scales and high capacities has become inevitable. This study aims to determine optimal locations and capacities for DG and ESS grid integration, maximizing benefits within distribution networks. A dual-layer planning model is developed, incorporating DWT, DPV joint output, and network clustering. The MIPSO algorithm, which exhibits strong adaptability, is proposed to solve the model's mixed-integer nonlinear characteristics. Test results demonstrate that the proposed method effectively addresses the planning challenge of DG-ESS grid integration, yielding significant improvements in both economic and operational aspects of the system. The results of the study are summarized as follows:

- A joint probability distribution model for DWT and DPV is established using the Frank-Copula function, considering the uncertainty and coupling characteristics of wind and solar power output in the distribution network.
- A cluster partitioning method based on electrical distance is developed to address the challenge of determining the number of DG and ESS interconnection nodes, significantly reducing the complexity of node selection.

- Case studies on the modified IEEE 33-bus system showed that integrating DG and ESS reduced annual comprehensive costs by 41.65%. Operationally, it mitigated voltage fluctuations by 24.35% and network losses by 55.72% daily, with energy storage subsidies increasing ESS penetration by 52.72%.

Given the continual rise in distribution network loads, strategic planning of DG-ESS within distribution networks is pivotal for their evolution and the integration of renewable energy sources. This study proposes effective solutions and strategies for determining optimal grid connection points and capacities for DG and ESS. However, opportunities for enhancement remain. Future research could concentrate on developing more sophisticated ESS models and scheduling strategies to optimize ESS longevity and profitability. Additionally, improving methods for addressing network losses, voltage fluctuations, and incorporating reactive power compensation methods are areas that warrant further investigation.

Acknowledgement: We thank our collaborators, anonymous reviewers, and the staff of the Energy Engineering journal for their contributions, feedback, and support, respectively. Special thanks go to the State Key Laboratory of Reliability and Intelligence of Electrical Equipment, Hebei University of Technology, for pivotal insights and essential resources.

Funding Statement: This research was funded by “Chunhui Program” Collaborative Scientific Research Project of the Ministry of Education of the People’s Republic of China (Project No. HZKY20220242) and the S&T Program of Hebei (Project No. 225676163GH).

Author Contributions: The authors confirm contribution to the paper as follows: study conception and design: Haoyuan Li, Lingling Li; data collection: Haoyuan Li, Lingling Li; analysis and interpretation of results: Haoyuan Li, Lingling Li; draft manuscript preparation: Haoyuan Li, Lingling Li. All authors reviewed the results and approved the final version of the manuscript.

Availability of Data and Materials: Data supporting this study are included within the article.

Ethics Approval: Not applicable.

Conflicts of Interest: The authors declare no conflicts of interest to report regarding the present study.

Nomenclature

h_x	Bandwidth for wind power kernel density estimation
λ	Parameter of the Copula that controls the strength of the correlation
S_{up}	Voltage magnitude-active power sensitivity matrix
S_{UQ}	Voltage magnitude-reactive power sensitivity matrix
D_{ij}	Overall impact of changes in the injected power at node i on the voltage magnitude at node j
L_{ij}	Electrical distance between node i and node j
N_k	Number of nodes in the k -th cluster
F_{upp}	Annual comprehensive cost of the distribution network, ¥
F_{op}	Annual operational costs, ¥
φ_{WT}	Operating costs of wind power, ¥/kW
φ_{PV}	Operating costs of PV power, ¥/kW
$P_{s,t}^{WT}$	Actual outputs of wind power at time t under scenario s , kW
$P_{s,t}^{PV}$	Actual outputs of PV power at time t under scenario s , kW
M_s	Number of typical scenarios divided into one year
η_s	Probability of the scenario in one year
φ_{ESS}	Operating cost of energy storage, ¥/kW
C_{WT}	Unit capacity investment costs of WT, ¥/kVA
C_{PV}	Unit capacity investment costs of PV, ¥/kVA
C_{ESS}	Unit capacity investment costs of ESS, ¥/kVA

F_{buy}	Cost of purchasing electricity from the upper-level grid, ¥/kW
R_{sell}	Revenue from selling electricity back to the upper-level grid, ¥/kW
E_t^{buy}	Grid electricity price at time t , ¥/kW
$E_{t,sub}$	Capacity price at time t , ¥/kW
φ_{loss}	Network loss discounting cost coefficient, ¥/kW
$P_{t,s}^{loss}$	System network loss power at moment t under scenario s , kW
φ_V	Voltage fluctuation penalty factor, ¥/kW
$V_{s,t,i}$	Voltage amplitude at node i at moment t under scene s
P_{DG_i}	Capacity of node i to access the DG, kW
P_{ESS_i}	Capacity of node i to access the DG, kW
$P_{k,DG}$	Planning capacity of DG in k clusters, kW
P_{load}	Total system load, kW
U_i	Voltage amplitude at node i
$P_{ESS,k}$	Maximum charging and discharging power of the ESS in cluster k , kW
η_t	Charging and discharging efficiency of ESS
$u_{e,k,t}$	Charging and discharging flag of the ESS
$SOC_{k,t}$	State of charge of the ESS in cluster k at time t
$S_{k,0}$	Initial state of charge of the ESS in cluster k

References

1. Pavel T, Polina S. Heterogeneity of the impact of energy production and consumption on national greenhouse gas emissions. *J Clean Prod.* 2024;434(3):139638. doi:10.1016/j.jclepro.2023.139638.
2. Lind L, Chaves-Ávila JP, Valarezo O, Sanjab A, Olmos L. Baseline methods for distributed flexibility in power systems considering resource, market, and product characteristics. *Utilit Policy.* 2024;86:101688. doi:10.1016/j.jup.2023.101688.
3. Sonnsjö H. What we talk about when we talk about electricity: a thematic analysis of recent political debates on Swedish electricity supply. *Ener Poli.* 2024;187:114053. doi:10.1016/j.enpol.2024.114053.
4. Shahbazi A, Aghaei J, Pirouzi S, Niknam T, Shafie-khah M, Catalão JPS. Effects of resilience-oriented design on distribution networks operation planning. *Elect Power Syst Res.* 2021;191(1):106902. doi:10.1016/j.epsr.2020.106902.
5. Paul S, Poudyal A, Poudel S, Dubey A, Wang Z. Resilience assessment and planning in power distribution systems: past and future considerations. *Renew Sustain Energy Rev.* 2024;189(10):113991. doi:10.1016/j.rser.2023.113991.
6. Ceylan O, Paudyal S, Pisica I. Nodal sensitivity-based smart inverter control for voltage regulation in distribution feeder. *IEEE J Photovolt.* 2021;11(4):1105–13. doi:10.1109/JPHOTOV.2021.3070416.
7. Venkateswaran VB, Saini DK, Sharma M. Approaches for optimal planning of energy storage units in distribution network and their impacts on system resiliency. *CSEE J Power Energy Syst.* 2020;6(4):816–33.
8. Cotilla-Sanchez E, Hines PDH, Barrows C, Blumsack S, Patel M. Multi-attribute partitioning of power networks based on electrical distance. *IEEE Trans Power Syst.* 2013;28(4):4979–87. doi:10.1109/TPWRS.2013.2263886.
9. Alkhayat G, Mehmood R. A review and taxonomy of wind and solar energy forecasting methods based on deep learning. *Energy AI.* 2021;4(7):100060. doi:10.1016/j.egyai.2021.100060.
10. Ben Ammar R, Ben Ammar M, Oualha A. Photovoltaic power forecast using empirical models and artificial intelligence approaches for water pumping systems. *Renew Energy.* 2020;153(5):1016–28. doi:10.1016/j.renene.2020.02.065.
11. Carvalho JH, Schwartz UB, Borges CLT. Copula based model for representation of hybrid power plants in non-sequential Monte Carlo reliability evaluation. *Sustain Ener, Grids Netw.* 2023;35(14):101077. doi:10.1016/j.segan.2023.101077.
12. Camal S, Teng F, Michiorri A, Kariniotakis G, Badesa L. Scenario generation of aggregated Wind, Photovoltaics and small Hydro production for power systems applications. *Appl Energy.* 2019;242(3):1396–406. doi:10.1016/j.apenergy.2019.03.112.

13. Lin S, Liu C, Shen Y, Li F, Li D, Fu Y. Stochastic planning of integrated energy system via frank-copula function and scenario reduction. *IEEE Transact Smart Grid*. 2022 Jan;13(1):202–12. doi:10.1109/TSG.2021.3119939.
14. Valencia A, Hincapie RA, Gallego RA. Optimal location, selection, and operation of battery energy storage systems and renewable distributed generation in medium-low voltage distribution networks. *J Energy Storage*. 2021;34(1):102158. doi:10.1016/j.est.2020.102158.
15. Bozorgavari SA, Aghaei J, Pirouzi S, Nikoobakht A, Farahmand H, Korpås M. Robust planning of distributed battery energy storage systems in flexible smart distribution networks: a comprehensive study. *Renew Sustain Energy Rev*. 2020;123(2):109739. doi:10.1016/j.rser.2020.109739.
16. Pemmada S, Patne NR, Ajay Kumar T, Manchalwar AD. Optimal planning of power distribution network by a novel modified jaya algorithm in multiobjective perspective. *IEEE Syst J*. 2022;16(3):4411–22. doi:10.1109/JSYST.2021.3132300.
17. Rastgou A. Distribution network expansion planning: an updated review of current methods and new challenges. *Renew Sustain Energy Rev*. 2024;189(1):114062. doi:10.1016/j.rser.2023.114062.
18. Fathabad AM, Cheng J, Pan K, Qiu F. Data-driven planning for renewable distributed generation integration. *IEEE Trans Power Syst*. 2020;35(6):4357–68. doi:10.1109/TPWRS.2020.3001235.
19. Behzadi S, Bagheri A. A convex micro-grid-based optimization model for planning of resilient and sustainable distribution systems considering feeders routing and siting/sizing of substations and DG units. *Sustain Cities Soc*. 2023;97(1):104787. doi:10.1016/j.scs.2023.104787.
20. Melaku ED, Bayu ES, Roy C, Ali A, Khan B. Distribution network forecasting and expansion planning with optimal location and sizing of solar photovoltaic-based distributed generation. *Comput Electr Eng*. 2023;110(6):108862. doi:10.1016/j.compeleceng.2023.108862.
21. Shoaie M, Noorollahi Y, Hajinezhad A, Moosavian SF. A review of the applications of artificial intelligence in renewable energy systems: an approach-based study. *Energy Convers Manag*. 2024;306(24):118207. doi:10.1016/j.enconman.2024.118207.
22. Pesaran HAM, Nazari-Heris M, Mohammadi-Ivatloo B, Seyedi H. A hybrid genetic particle swarm optimization for distributed generation allocation in power distribution networks. *Energy*. 2020;209(12):118218. doi:10.1016/j.energy.2020.118218.
23. Xu X, Niu D, Peng L, Zheng S, Qiu J. Hierarchical multi-objective optimal planning model of active distribution network considering distributed generation and demand-side response. *Sustain Energy Technol Assess*. 2022;53(6):102438. doi:10.1016/j.seta.2022.102438.
24. Tee WH, Gan CK, Sardi J. Benefits of energy storage systems and its potential applications in Malaysia: a review. *Renew Sustain Energy Rev*. 2024;192(7):114216. doi:10.1016/j.rser.2023.114216.
25. Si S, Sun W, Wang Y. A decentralized dispatch model for multiple micro energy grids system considering renewable energy uncertainties and energy interactions. *J Renew Sustain Ener*. 2024;16(1):015301. doi:10.1063/5.0192716.
26. D'Adamo I, Dell'Aguzzo A, Pruckner M. Residential photovoltaic and energy storage systems for sustainable development: an economic analysis applied to incentive mechanisms. *Sustain Dev*. 2024;32(1):84–100. doi:10.1002/sd.2652.
27. Ranjbar H, Saber H. A risk-aware and second-order cone programming model for wind expansion planning considering correlated uncertainties using the copula method. *Sustain Ener Grids Netw*. 2024;38(21–22):101307. doi:10.1016/j.segan.2024.101307.
28. Gad AG. Particle swarm optimization algorithm and its applications: a systematic review. *Arch Comput Methods Eng*. 2022;29(5):2531–61. doi:10.1007/s11831-021-09694-4.
29. Hassanat A, Almohammadi K, Alkafaween E, Abunawas E, Hammouri A, Prasath VBS. Choosing mutation and crossover ratios for genetic algorithms—a review with a new dynamic approach. *Information*. 2019;10(12):390. doi:10.3390/info10120390.

30. Kumar A, Kumar A, Mallipeddi R, Lee D-G. High-density cluster core-based k-means clustering with an unknown number of clusters. *Appl Soft Comput.* 2024;155(5):111419. doi:10.1016/j.asoc.2024.111419.
31. Hannan MA, Wali SB, Ker PJ, Rahman MSA, Mansor M, Ramachandramurthy VK, et al. Battery energy-storage system: a review of technologies, optimization objectives, constraints, approaches, and outstanding issues. *J Energy Storage.* 2021;42:103023. doi:10.1016/j.est.2021.103023.